Eur. Phys. J. A **7**, 367–375 (2000)

THE EUROPEAN PHYSICAL JOURNAL A

Reaction mechanism of ^{6}Li scattering at 600 MeV

K. Schwarz[1,2], C. Samanta[1,3], M. Fujiwara[1,6], H. Rebel[2], R. De Leo[4], N. Matsuoka[1], H. Utsunomiya[5], H. Akimune[6], I. Daito[1], H. Fujimura[1], F. Ihara[1], K. Ishibashi[1], Y. Maeda[1], T. Yamanaka[1], H. Yoshida[1], A. Okihana[7], T. Yoshimura[7], P.K.J. van Aarle[1,8], W.A.T. Uijen[1,8], M. Ito[9], Y. Sakuragi[9]

[1] Research Center for Nuclear Physics, Osaka University, Osaka 567-0047, Japan
[2] Institut für Kernphysik, Forschungszentrum Karlsruhe, 76021 Karlsruhe, Germany
[3] Saha Institute of Nuclear Physics, 1/AF Bidhannagar, Calcutta 700 064, India
[4] University of Bari, Dipartimento di Fisica, 70126 Bari, Italy
[5] Konan University, Kobe, Japan
[6] Advanced Science Research Center, Japan Atomic Energy Research Institute, 2-4 Tokai, Ibaraki 319-1195, Japan
[7] Kyoto University of Education, Kyoto, Japan
[8] Eindhoven University of Technology, 5612 AZ, Eindhoven, The Netherlands
[9] Department of Physics, Osaka City University, Osaka 558-8585, Japan

Received: 17 December 1999 / Revised version: 9 February 2000
Communicated by D. Schwalm

Abstract. Elastic scattering and inclusive breakup of ^{6}Li particles on ^{12}C, ^{58}Ni, ^{90}Zr, and ^{208}Pb targets are measured at 100A MeV. The elastic scattering data are compared with single channel and Coupled Discretized Continuum Channels calculations. The coupling-effect between the elastic and the breakup channels is important even at an incident energy of 100A MeV and cannot be neglected. The inclusive breakup data are investigated for orbital dispersion effects which are found to be less significant at 100A MeV. The longitudinal momentum distributions are broader than predicted by theoretical expectations.

PACS. 24.50.+g Direct reactions – 25.60.Gc Breakup and momentum distributions – 27.20.+n $6 \leq A \leq 19$

1 Introduction

Nuclear reactions of energetic projectiles with low breakup thresholds are currently investigated with new vigour in view of possible access to fusion reactions of astrophysical interest at stellar energies [1]. Due to the particular nuclear structure of the ^{6}Li nucleus, ^{6}Li induced reactions provide a unique possibility to study specific features of the nuclear reaction mechanism, in particular the role of breakup processes and their feedback to other reaction channels [2–4]. A remarkable feature of ^{6}Li scattering in the energy range of some ten MeV, noticed in the seventies, is the failure of the double-folded potential in explaining the elastic scattering data in a one step reaction mechanism [5]. Coupled Discretized Continuum Channels (CDCC) studies [2] have shown that the breakup effect is the key to understanding the experimental cross sections in the low-energy region, where a strong coupling appears between the elastic and the breakup channels. This coupling effect is expected to decrease with increasing incident energy, which is understood as the result of a weaker nucleon-nucleon interaction and a shorter transit time of the projectile.

The basic breakup-mechanism can be described by the participant-spectator model [6] in which one of the particles of the projectile acting as a participant strikes the target nucleus while the other misses and retains its forward momentum, acting as a spectator and travels on practically undisturbed. This implies a velocity distribution of the spectator-particles which results from a superposition of the beam-velocity with the internal motion of the fragments inside the projectile. It has been found that the longitudinal momentum distribution directly reflects the internal momentum distribution of the clusters within the projectile whereas the transverse momentum distribution is affected by the projectile-target interaction [7,8].

In a CDCC study at E_{lab} = 100A MeV using the cluster folding model (CFM) interaction [9], a decoupling of the breakup-channels and the elastic reaction channel was predicted to occur at intermediate energies [10]. In the CFM potentials the medium effect of the nuclear interaction such as the energy and density dependence is not fully taken into account. Furthermore the CFM potential depth considerably decreases at intermediate energies due to a rapid decrease of the strength of V_α and V_d, which in turn induces a rather small coupling potential and therefore causes negligible coupling effects on

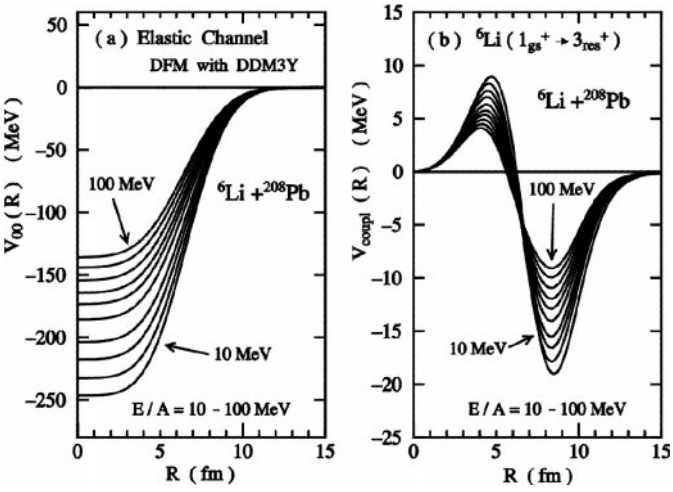

Fig. 1. Energy dependence of DFM potentials with DDM3Y interaction of the ^{6}Li+^{208}Pb system in the energy range of E_{lab} = 10A - 100A MeV in steps of 10 MeV, (a) for the diagonal potentials, and (b) for the coupling potentials between the ground state and the 3^+ resonant state of ^{6}Li at E_x = 2.186 MeV. The potential strengths decrease monotonically with the energy in both cases

the elastic scattering [10]. There is also some indication that a CFM description with an a-priori introduced cluster structure may absorb the coupling effect [11]. In fact, recent theoretical investigations of the projectile-breakup effect on ^{6}Li elastic scattering using CDCC calculations with a potential constructed from the DDM3Y interaction [12] in a double folding model (DFM) show that the breakup effect becomes less important, although it is not completely negligible even at E_{lab} = 100A MeV [13]. The decrease of the breakup effect with increasing energy can be understood as being due to the decrease of the coupling potentials for the breakup channels. Figure 1 shows the energy dependence of the diagonal potential in the elastic channel (left) and that of the coupling potential between the elastic channel and the 3^+-resonance channel (right) in the energy range of E_{lab} = 10A - 100A MeV. Since the breakup effect on the elastic scattering is a process of second and higher order, one can say that the coupling effect decreases roughly two times as quick as the DFM interaction potentials itself.

Also theoretical studies dealing with elastic scattering of the loosely bound deuteron at incident energies up to 350A MeV, compared with experimental data, show that the breakup effect at high energies does not become negligible [14,15].

^{6}Li + nucleus elastic scattering data exist up to 53A MeV incident energy [16]. These data have been studied earlier in a CDCC framework and a considerable breakup channel coupling effect has been found at low energy [3, 13]. In order to study the role of the breakup channels and its feedback to the elastic scattering at intermediate energy, the elastic differential cross sections of 100A MeV ^{6}Li scattered on various nuclei as well as the breakup bumps in the inclusive energy spectra of the breakup fragments are presented.

2 Measurement

The cross sections of elastic ^{6}Li scattering on ^{208}Pb (12.99 $\frac{mg}{cm^2}$), ^{90}Zr (7.34 $\frac{mg}{cm^2}$), ^{58}Ni (5.86 and 4.00 $\frac{mg}{cm^2}$) and ^{12}C (4.1 and 30 $\frac{mg}{cm^2}$) have been measured from Θ_{lab} = 3° to 14.5°. The measurements also include the angular distribution of the breakup fragments α-particles and deuterons from Θ_{lab} = 4.5° to 14.5° as well as the full region of the breakup bumps in the inclusive energy spectra of the breakup fragments α-particles, deuterons, tritons and ^{3}He-particles at Θ_{lab} = 5.5°. Self-supporting target foils have been bombarded by ^{6}Li-ions with an energy of E_{lab} = 100A MeV which were accelerated by the RCNP Ring Cyclotron. The beam has been stopped by a Faraday cup in the scattering chamber. A typical beam intensity has been 1 nA. The charged particle spectra have been measured with the magnetic spectrometer "Grand Raiden" [17]. This QQDD-type spectrometer provides a good angular resolution for the scattered particles of roughly 0.17° in horizontal direction and 0.57° in vertical direction. The focal plane detector consists of two multi-wire drift chambers providing the momentum information by measuring the position in the focal plane. Two additional plastic scintillators, measuring the energy loss ΔE and the residual energy E are used for particle identification. The spectrograph has been rotated in steps of 1.5° starting from 3°. Several measurements have been taken with a certain angular overlap. It has been possible to connect all measurements smoothly and to obtain complete angular distributions in the whole measured range.

The broad breakup bumps of α-particles, deuterons, ^{3}He and tritons have been measured in a similar way. Since the momentum acceptance of the spectrometer Grand Raiden for one magnetic field setting is not sufficient to cover the whole shape of the breakup bumps, several overlapping settings have been used. These measurements have been done at an angular position of 5.5° for all targets (^{208}Pb,^{90}Zr,^{58}Ni and ^{12}C).

3 Elastic Scattering of ^{6}Li and Channel Coupling

The method of Coupled Discretized Continuum Channels is a phenomenological method of analysing direct nuclear reactions which in particular involve breakup of loosely bound particles. A major problem in the application to breakup processes is that the breakup states are in the continuum and one has to consider an infinite number of coupled channels. A method of treating the continuum channels has been given by [18] who used the so called "method of momentum bins". In this method the momentum space of the internal motion of the potential breakup fragments inside the projectile is divided into a finite number of bins in which the internal wave functions are averaged. By this way the continuum can be replaced by a

finite number of discretised "channels". For realistic calculations a model space has to be specified by the maximum linear and angular momenta of the relative motion between the clusters within the projectile, k_m and l_m respectively, and the size of the bin, Δk, or equivalently the number of discretised channels N for a given k_m. The adequacy of the model space has to be tested for convergence of the calculated transition matrix elements with respect to an increase of k_m, l_m or N [19]. The idea is to treat the reaction channels in which the projectile stays in the ground state and the reaction channels in which the projectile goes into excited states simultanously with the coupled-channels method. In the cluster-folding model (CFM) the diagonal and coupling form factors are calculated by folding the optical potentials of the breakup fragments into the wave functions of the projectile ground and discretised continuum states. Alternatively the double-folding model (DFM) folds an effective nucleon-nucleon interaction (M3Y or DDM3Y) with the target ground-state density and with the diagonal or transition densities of the projectile nucleus. These calculations were first developed for deuteron breakup. Details of the CDCC method can be found in [2,20,21]. It was found that in deuteron-breakup-processes transitions among excited channels themselves (continuum-continuum-coupling) are much stronger than those between the ground state channel and the individual excited channels (bound-continuum-coupling). The deuteron breakup has been found to proceed dominantly via multistep processes. [20]. A similar finding has been made for the case of ^{6}Li breakup, where the continuum s-wave states couple mainly in an indirect way via the resonant 2^+ and 3^+ d-wave states to the ground state. This implies that the full coupled channel multi-step process can be hardly well approximated by one-step process DWBA calculations [22].

In the present CDCC-calculations for the elastic scattering cross section the contribution of the breakup mode to the scattering potential is studied. We take into account the coupling to the ^{6}Li $\rightarrow \alpha$+d continuum channels with the α-d relative momentum, k, up to 1.0 fm^{-1}. Among the excited states we find that the coupling to the S-wave (ℓ=0) continuum and the D-wave (ℓ=2) resonance states, 3^+, 2^+ and 1^+ at excitation energies of 2.186 MeV, 4.31 MeV and 5.65 MeV respectively, have a dominant contribution to the elastic scattering and, as far as the effect on the elastic scattering is concerned, the coupling to other parts of continuum states is almost negligible. In the practical CDCC calculations we have discretised the S-wave continuum into four bins. This model space for the breakup states is the same as that adopted in the references [10] and [13]. Since the channel coupling in case of a ^{6}Li projectile occurs due to its low lying α-d breakup threshold (1.475 MeV) the ^{3}H-^{3}He breakup should have a significantly reduced importance in this connection because of the larger energy transfer involved.

A relativistic kinematics has been used throughout the CDCC calculations presented here. The projectile target interaction potentials have been calculated by using a double folding model (DFM). The DFM used here is a realistic density- and energy-dependent generalisation of the M3Y effective nucleon-nucleon interaction [23] called DDM3Y. The DFM based on the DDM3Y relates the differential cross section more directly to the shape of the interacting nuclei [24] with explicit consideration of the projectile-target density distributions. Strictly, the shape of the imaginary potential (accounting for reaction channels not explicitly coupled) is expected to be different [25] from that of the real part. In the present analysis, for sake of simplicity we adopted the procedure to take the absorptive part proportional to the real potential (derived from the DDM3Y interaction) by a factor N_I. This simplification could be the origin for an imperfect reproduction of the data, but provides an estimate of the strength of the imaginary part, when the most important breakup channels are explicitely treated. Recently for the case of deuteron scattering the contribution of the elastic and nonelastic breakup channels to the imaginary potential has been theoretically calculated on the basis of the post form DWBA [22]. There are also detailed experimentally based results for the reaction of 156 MeV ^{6}Li + ^{40}Ca available, which reveal the dominant contribution of the nonelastic channel to the total breakup cross section [26]. It would be of interest to compare theoretical estimates for 100A MeV ^{6}Li scattering with the present results.

Figure 2 compares CDCC calculations with the ^{6}Li scattering data. The above mentioned strength factor N_I is the only adjusted parameter (for some details see also [13]). For all targets a best fit to the elastic scattering data results in a value of $N_I = 0.63$. Only for the ^{12}C target a lower value has been found to be significant. This indicates a weaker absorption and the refraction of the real potential. But even with $N_I = 0.4$ the experimental data to the ^{12}C target are not well fitted in the angular region with $\Theta_{cm} \geq 15°$. This may be a hint that there is still some room for improving the DFM potential using the present version of DDM3Y interaction itself. Another possible reason for the failure of the CDCC calculation to fit the data on the ^{12}C target may be the constraint by the shape of the imaginary potential being identical to the real part. The sharp dips appearing in the theoretical calculations for the heavier targets are not observed experimentally due to finite angular resolution of the spectrometer.

We have also investigated the effect of target excitations in the case of the ^{12}C target and it has been found that it is completely negligible as compared with the ^{6}Li breakup effect. For the other targets the same effect is expected to be even less since all of them are closed shell nuclei.

To a certain extent the breakup effect could be simulated by single-channel calculations with a renormalised real DFM potential. A DFM potential reduced by about 10% can reproduce the CDCC results at 100A MeV, but only in the forward angle region (up to $\sim 10°$), irrespective of the targets. At 35A MeV this reduction factor has been about 25% [3], indicating stronger coupling at lower incident energy. Since single-channel calculations with renormalised DFM potentials do not reproduce the CDCC results in the whole angular region, the dynamic polarisation

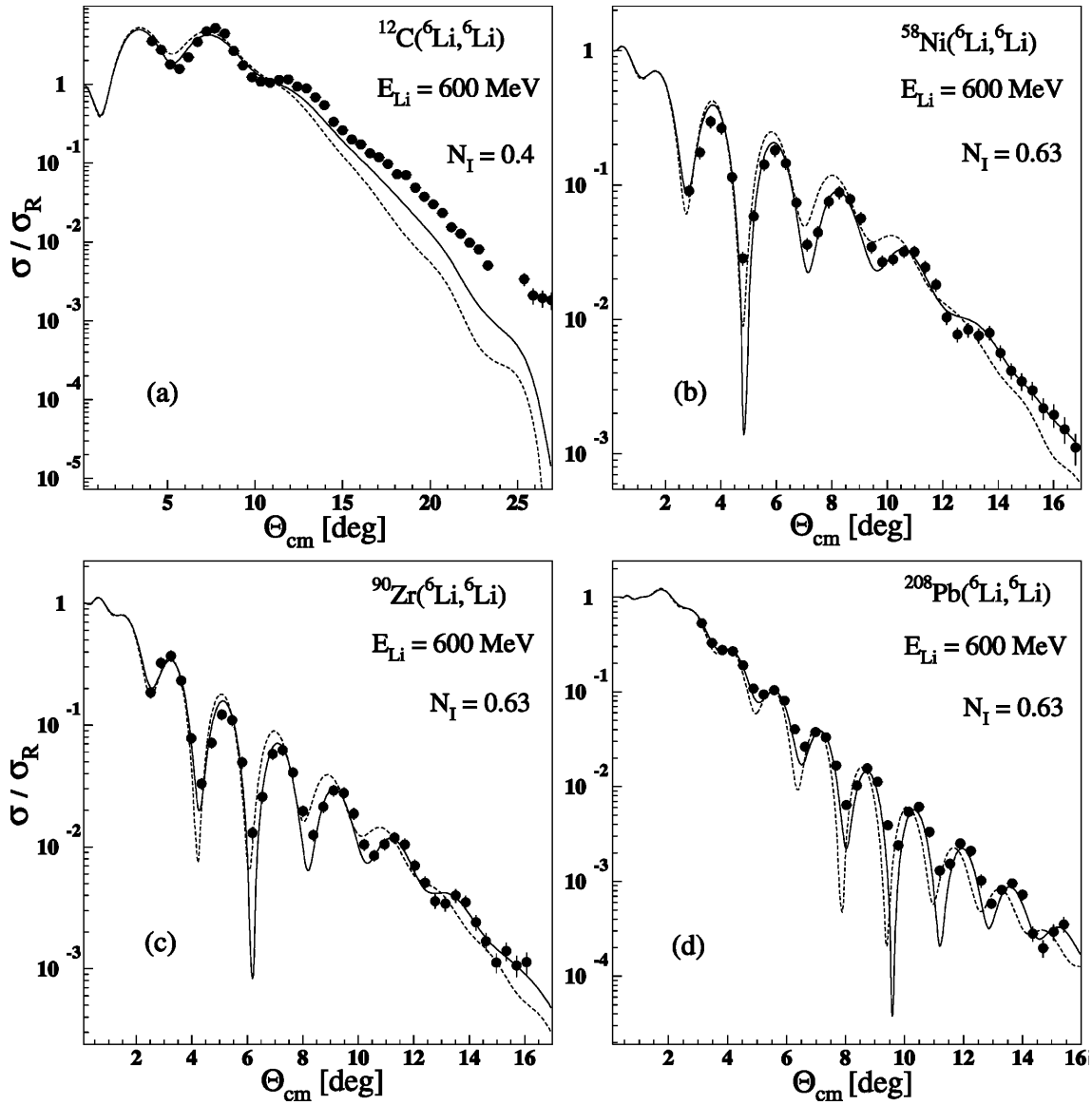

Fig. 2. Angular distributions of ^{6}Li scattering from different targets compared with CDCC (solid lines) and single channel (dotted lines) calculations using a DFM potential with DDM3Y effective interaction. No renormalisation of the real part of the DFM potential is made. For the imaginary part of the potential, the strength factor N_I is given

potential which is induced by virtual projectile excitations would not simply be proportional to the DFM potential. An example of the contribution to the real part has been found in the scattering of ^{6}Li ions. In this case the coupling of the projectile breakup channels (dominantly of the α-d resonant channels) with the elastic channel is very strong and induces a surface-peaked repulsive potential [2,3,27] which amounts to about a half of the diagonal potential of the elastic channel with the opposite sign. The characteristic feature of the dynamic polarisation potential induced by a specific excited channel has been understood to be governed by the ratio of the imaginary part of the coupling potential to its real part. For ^{6}Li scattering this ratio has been found to be 0.6 which brings out a real part of the dynamic polarisation potential being strongly repulsive and an imaginary part which is almost equal to zero. More details can be found in [2,20,28]. We have succeeded in simulating the CDCC result by the single-channel calculation by adding a surface peaked Woods-Saxon derivate ΔV to the DFM potential V_{DF} described as follows: $U_{op} = (V_{DF} + \Delta V) + iN_I V_{DF}$. Such a detailed shape of the dynamic polarisation potential has been already described in [27].

In case of the ^{58}Ni target we also have been able to perform comparative CDCC calculations by using the cluster folding model (CFM) interaction. As can be seen in Fig. 5 of [13], the peak positions in the CFM calculations are shifted towards smaller angles. This dissimilarity seems to come mainly from the difference of the radial shape of the potentials calculated on basis of different folding model procedures. The CFM potential is also deeper than the DFM potential by more than 10% [13]. Since the CFM po-

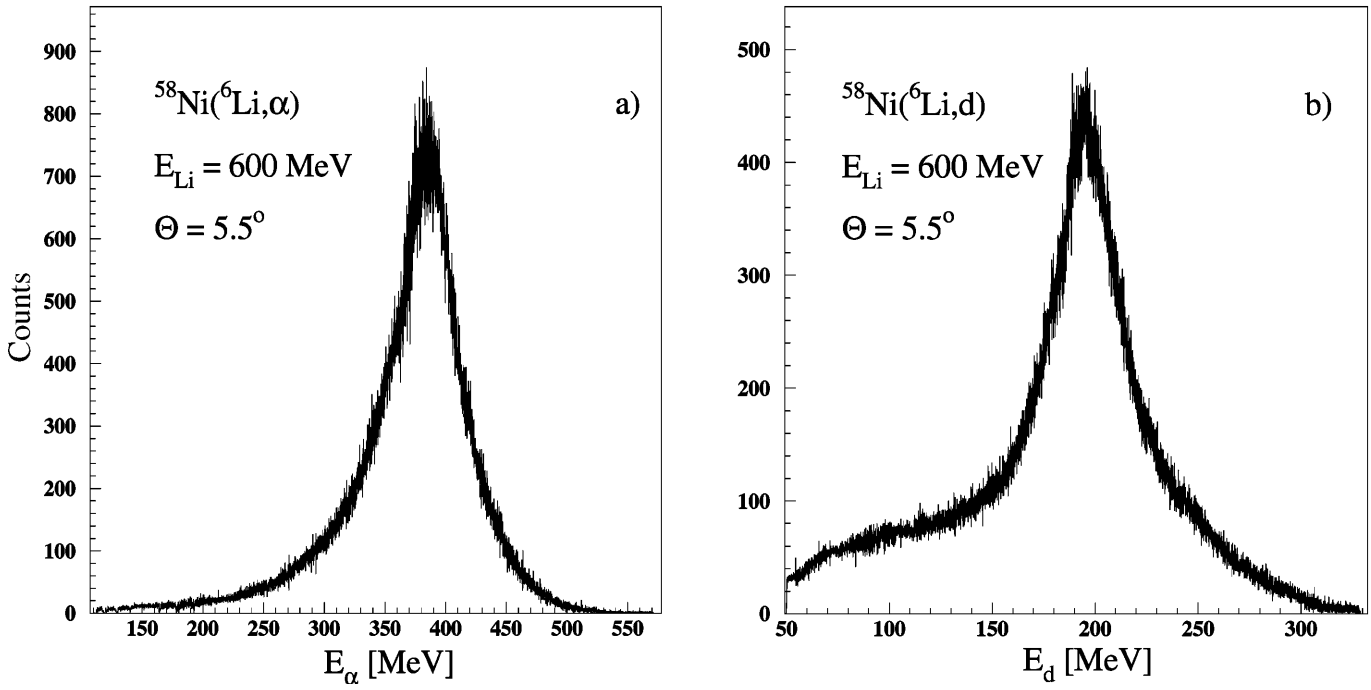

Fig. 3. Inclusive energy spectra of α-particles and deuterons from 100A MeV ^{6}Li breakup on ^{58}Ni target. The Peaks of the breakup bumps correspond to double differential cross section values of 28.3 $\pm$2.7$\frac{mb}{sr-MeV}$ for α-particles and 24.8 $\pm$2.4$\frac{mb}{sr-MeV}$ for deuterons, respectively. Both values have been determined for an energy intervall of 15 MeV

tentials are only applicable when empirical optical potentials for the α-particle and deuteron clusters are available on a particular target nucleus at a particular incident energy, CFM-model calculations for other targets could not be done.

4 Analysis of the Inclusive Breakup

Whenever the kinetic energy of a complex nuclear projectile is considerably larger than the binding energy of its constituents, fragmentation or breakup processes play an important role in nucleus-nucleus collisions. This phenomenon is signalled by broad bumps in the continuum part of the inclusive energy or momentum spectra of the emitted particles. As can be seen in Fig. 3, these bumps basically have a Gaussian shape and are centered around the beam velocity. But the mean energy is slightly downshifted by $E_0 \sin^2(\theta)$ + Q-value + energy loss in the target. A low energy tail can be observed which has been interpreted at 156 MeV as a physical background coming from precompound and compound nuclear reactions [29].

As mentioned above the longitudinal momentum distribution has been found to reflect the internal momentum distribution of the clusters within the projectile whereas the transverse momentum distribution has been found to be affected by the projectile-target interaction [7,8]. Since the mentioned investigations have been done either with heavier projectiles and fragments or by using a much lower energy, our own data shall be presented here based on 100A MeV ^{6}Li projectiles.

For the ^{12}C target the complete inclusive α-particle breakup bump at $\Theta_{lab} = 5.5°$ has been measured as well as the central part of the bump at several angles. For each angle from $\Theta_{lab} = 4°$ to 8.5° the double differential cross section $d^2\sigma/d\Omega dE$ has been determined. When written as

$$\frac{d^2\sigma}{d\Omega dE} = P(\mathbf{p})\frac{m_a p_a}{(2\pi\hbar)^3}$$

with P($\mathbf{p}$) being the estimated momentum distribution and assuming a Gaussian distribution in both p_p and p_t by expressing

$$P(\mathbf{p}) = k \;\; exp(-p_p^2/2\sigma_p^2 - p_t^2/2\sigma_t^2)$$

the data can be fitted in a two parameter fit. In these formulas k is a normalisation constant, p_a the α-particle momentum in the laboratory system, m_a the α-particle mass, p_p the internal longitudinal momentum and p_t the internal transversal momentum carried by the α-particles. The quantities σ_p and σ_t are the longitudinal and transverse momentum distribution widths. In the following way it has been possible to determine all parameters of the formula given above. First for an $\mathbf{p}_p = 0$, which means for the central momentum of the breakup bump, the double differential cross section is plotted against p_t of all angles which are included in the analysis. The experimental data are fitted with a Gaussian function by using the above mentioned formulas, but for an $\mathbf{p}_p = 0$, which simplifies the expression to

$$P(p_t; p_p = 0) = k \;\; exp(-p_t^2/2\sigma_t^2).$$

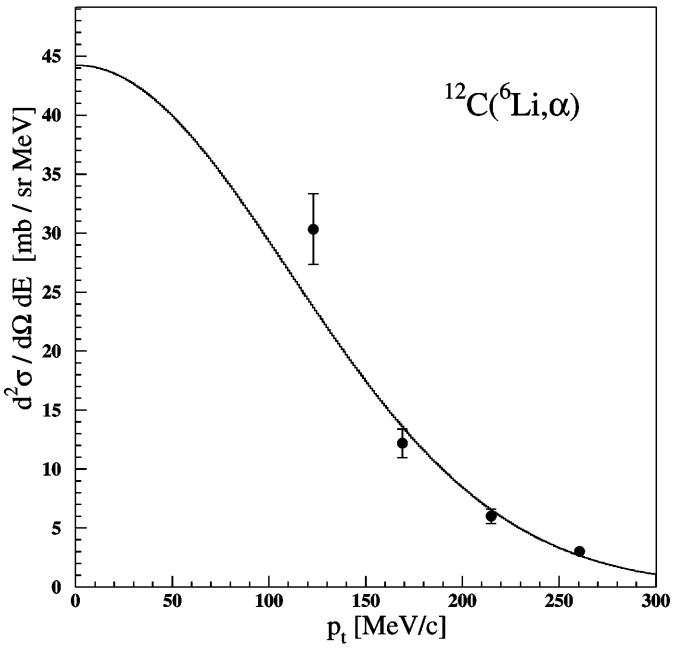

Fig. 4. Double differential cross section plotted against p_t. Included are data from $\Theta_{lab} = 4°$ to 8.5°. Each p_t value corresponds to one scattering angle. The experimental data are fitted with a Gaussian function

The fit results in a transverse momentum distribution width of $\sigma_t = 110.35$ MeV/c and a normalisation constant $\tilde{k} = k/(2\pi\hbar)^3 = 0.55 \times 10^{-5}\ \frac{mb}{sr(MeV/c)^3}$ (Fig. 4).

Subsequently the transversal momentum value is fixed at an angle of $\Theta_{lab} = 5.5°$ which is the angle at which most of our inclusive data have been taken. The longitudinal momentum is varied over the full momentum range of the complete α-particle breakup bump and a graph is created with the resulting double differential cross sections plotted against the longitudinal momentum distribution p_p. These experimental data points are fitted by using a Gaussian function representing the real breakup events plus a background function representing mainly a continuum due to preequilibrium emission and possible higher order processes [30] . The shape of the used background function is similar to the one found by Neumann et al. [31] in the frame of the coalescence model and can be parameterised as the product of a Breit-Wigner and a cutoff function $f = N(1 - exp[(E - E_0)/a])/(1 + [(E - E_1)/b]^2)$ [32]. The fit results in Gaussian parameters of $\sigma_p = 88.95$ MeV/c and a normalisation constant which is in reasonable agreement with the normalisation factor acchieved from the transverse momentum distribution. A similar procedure is carried through for the case of the ^{208}Pb target. Here the two parameter fit described above results in a normalisation factor $\tilde{k}$ of 6.34×10^{-5}, a $\sigma_t = 103.79$ MeV/c, and a σ_p of 76 MeV/c. For the remaining two targets, namely ^{58}Ni and ^{90}Zr, inclusive breakup data are only available at $\Theta = 5.5°$. This means that a transverse momentum distribution could not be acchieved and only the longitudinal momentum distribution could be analysed. Fits result in $\sigma_p = 86.96$ MeV/c (^{58}Ni) and $\sigma_p = 86.85$ MeV/c (^{90}Zr). The double differential cross sections plotted over p_p and the corresponding fits for all four targets are displayed in Fig. 5. The resulting fit parameters are listed in Table 1. In the last row also the impact parameters are displayed.

5 Discussion of the Momentum Distributions

Basically it has been expected that the variance of the longitudinal momentum distribution should not vary significantly when comparing different targets since it should reflect the original internal momentum distribution in the ^{6}Li-projectile. This can be observed when comparing the first three targets (^{12}C, ^{58}Ni, and ^{90}Zr). But the FWHM of the longitudinal momentum distribution in case of the ^{208}Pb target seems to be significantly smaller than for the other three targets. One possible reason could be found in the impact parameters for $\Theta_{lab} = 5.5°$ and an incident energy of 600 MeV which are significantly smaller than the nuclear radius in case of the three lighter targets (C, Ni, and Zr). Only for the ^{208}Pb target the impact parameter is in the border region of the nucleus. This could mean that the momentum distribution in case of the first three targets does not only reflect the internal Fermi motion of the clusters within the projectile but shows also an additional broadening by interaction with the nucleus. This effect would not be visible in the case of the low energy scattering presented in [7] where only Coulomb scattering takes place.

Under the assumption of independently moving nucleons forming the projectile Goldhaber [33] has found that the variance of the longitudinal momentum distribution of the fragment is given by

$$\sigma_p^2 = \sigma_0^2 \frac{b(a-b)}{a-1},$$

where a and b are the projectile and fragment mass numbers. σ_0 is dependent on the internal Fermi motion and at an incident energy of 92.5A MeV it has been found to be 80 MeV/c in case of Au target and 86 MeV/c for Al target [8] or 86 MeV/c at 2.1A GeV, averaged over many targets [34]. The σ_0 derived from our experimental values for σ_p are $\sigma_0 = 69.24$ MeV/c, averaged over the three lighter targets, and 60.1 MeV/c for $\sigma_p = 76$ MeV/c or 49.8 MeV/c for a σ_p of 63 MeV/c in case of the ^{208}Pb target. We find that they are by about 20 to 25% lower than the values found by Bibber *et al.* [8]. But in both cases the σ_0 derived from heavier targets (Au and Pb) are smaller than the ones derived from lighter targets (Al, C, Ni, Zr). Also our σ_0 are significantly higher than the value found by Srivastava *et al.* [7] for ^{12}C target and an incident energy of 26A MeV, which is only σ_0=28.6 MeV/c. According to Srivastava *et al.* [7] this low value for σ_0 indicates a change of the breakup reaction mode from transfer to fast abrasion-ablation processes. When comparing with the σ_0 of 86 MeV/c found for an incident energy of 2.1A GeV and the value found by Srivastava *et al.* it is plausible that our value, measured at an energy of 100A MeV, lies in between both values. But the difference to the σ_0 of

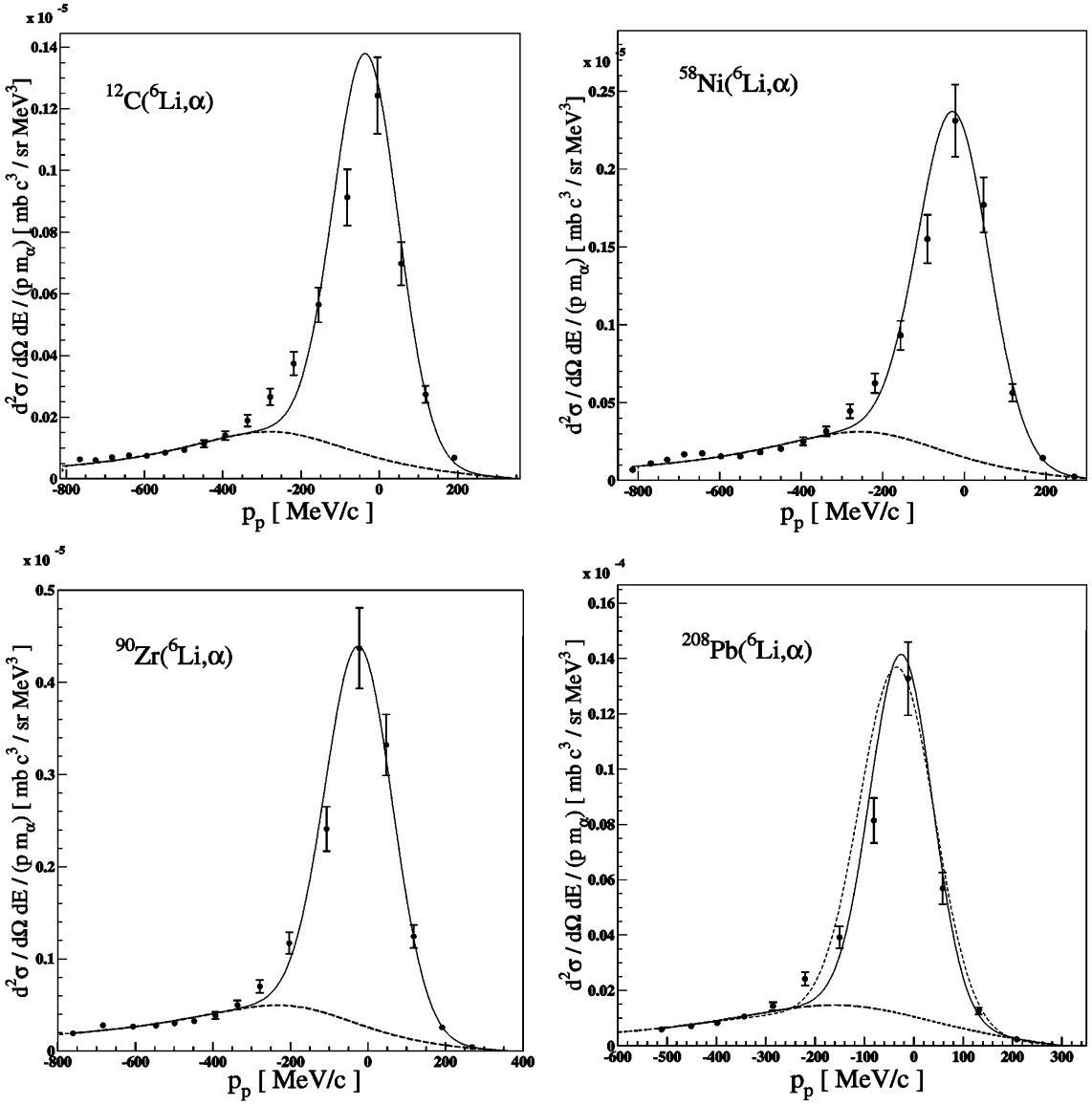

Fig. 5. Double differential cross section plotted against p_p. Displayed are data taken with ^{12}C, ^{58}Ni, ^{90}Zr, and ^{208}Pb targets at $\Theta_{lab} = 5.5°$. For each target the experimental values have been fitted independently by using a Gaussian function plus a parameterised background function. For the ^{208}Pb target two fits are displayed. One with $\sigma_p = 63$ MeV/c (solid line) and one with $\sigma_p = 76$ MeV/c (dashed line)

Bibber *et al.* [8], which has been determined at an almost identical energy, might be a hint that there is still room for investigation.

In Fig. 6 a comparison of the experimentally found σ_p for the case of the ^{208}Pb target with a theoretical distribution up to where an approximation by a Gaussian shape can be done is shown. All functions are normalised to unity. To achieve a better agreement with the theoretical momentum distribution we have fitted not only a Gaussian function with a $\sigma_p = 76$ MeV/c to the experimental data ($\chi^2 = 5.2$) but also a Gaussian function with a σ_p of 63 MeV/c ($\chi^2 = 3.4$) which is even in better agreement with the data of the longitudinal momentum distribution. But for the smaller σ_p a common normalisation factor with the transverse momentum distribution could not be found. This has been possible only for the larger σ_p of 76 MeV/c. Technically the ^{208}Pb data could even be fitted with a χ^2 of 9.1 by using the momentum distribution derived from the cluster wave function of Sakuragi *et al.* [2] plus a background function. It can be seen that the width of the displayed cluster wave function derived by Sakuragi *et al.* is smaller than the widths of both distributions fitted to the experimental data. Even the Gaussian function with the smaller σ_p is still significantly broader than the theoretical function.

For a description of the variance of the transversal momentum distribution the formula of Goldhaber should be modified [8]. The origin of the larger widths may be understood due to the orbital deflection of the projectile before fragmentation takes place. Since a wide range of impact

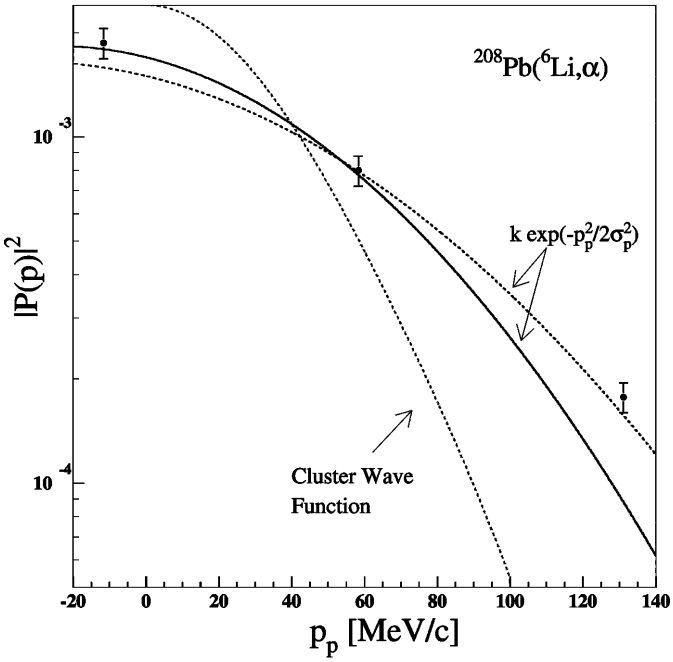

Fig. 6. Comparison of a theoretical cluster momentum distribution with the observed longitudinal momentum distributions (parameterised in a Gaussian form). The solid line corresponds to the curve with $\sigma_p = 63$ MeV/c and the dashed line to the curve with $\sigma_p = 76$ MeV/c. All functions are normalised to unity

parameters contribute to the breakup-cross section, the orbital deflection gives an additional contribution to the transverse momentum. Thus, by considering the dispersion due to the orbital deflection of the projectile by the Coulomb-nuclear field of the target the modification of the Fermi motion can be understood. An extension of the original Goldhaber formula is [8]:

$$\sigma_t^2 = \frac{b(a-b)}{a-1}\sigma_0^2 + \frac{b(b-1)}{a(a-1)}\sigma_D^2,$$

where the first term represents the intrinsic nucleon motion and σ_D in the second term is the variance of the transverse momentum of the projectile at the time of fragmentation. The parameters a and b are again the mass numbers of projectile and fragment [8].

Using the above formula we find σ_D =103.26 MeV/c for ^{12}C and 111.77 or 130.41 MeV/c for ^{208}Pb. When comparing with the values of Srivastava *et al* [7] ($\sigma_D = 22.8$ MeV/c for ^{12}C and $\sigma_D = 153.1$ MeV/c for ^{208}Pb) which have been determined for a much lower incident energy it can be seen that the σ_D for Pb are in the same order of magnitude (ours is smaller by 15 to 27%) whereas the σ_D for ^{12}C differ significantly. The σ_D found by Srivastava *et al.* for the ^{12}C target is much smaller than the value deduced from our experimental data. Also it might be interesting that the σ_t found by Srivastava *et al.* for the Pb target ($\sigma_t = 103.7$ MeV/c) is absolutely identical to the one found by us. When comparing our parameters with the values of Bibber et al. [8] (σ_D between 169.6 and 197.2 MeV/c), which have been determined for a similar incident energy (92.5A MeV to 117.5A MeV) but deduced from heavier projectile breakup (^{16}O instead of ^{6}Li) it shows that our values are much smaller. According to [8] the additional contribution of σ_D to the width of σ_t should become more important the lower the energy of the projectile is. At 1.05A GeV the orbital dispersion term should practically vanish entirely. Thus it may be understood that the differences between σ_p and σ_t in our case is by far not as large as it is in the case of [7] for the ^{208}Pb target. But on the other hand, the difference between σ_p to σ_t in the case of Bibber *et al.* is significantly larger than the difference found by us even when comparing comparably heavy targets (Pb and Au) and comparable incident energies. Table 1 compiles the results for the momentum distributions.

Table 1. Parameters for the longitudinal and transverse momentum distributions of breakup α-particles for an incident energy of 100A MeV of the ^{6}Li projectile. The values in brackets in case of the Pb target correspond to the second fit with smaller σ_p (see also text). In the last row the impact parameters for a scattering angle of $\Theta = 5.5^\circ$ are displayed

	^{12}C	^{58}Ni	^{90}Zr	^{208}Pb
σ_p [MeV/c]	88.95	86.96	86.85	76 (63)
σ_t [MeV/c]	110.35			103.79
σ_0 [MeV/c]	70.32	68.75	68.66	60.08 (49.81)
σ_D [MeV/c]	103.26			111.77 (130.41)
$\tilde{k}$ $[\frac{mb}{sr(MeV/c)^3}]$	0.55×10^{-5}			6.34×10^{-5}
b [fm]	0.45	2.09	2.99	6.15

6 Conclusion

The fragmentation of ^{6}Li into α-particle and deuteron is observed as a prominent reaction channel at 100A MeV. The effect of the breakup on the 100A MeV ^{6}Li elastic scattering on ^{12}C, ^{58}Ni, ^{90}Zr, and ^{208}Pb targets has been studied in a Coupled Discretised Continuum channels framework in which the resonant and non-resonant breakup channels are coupled with the elastic one [13]. The CDCC calculations using the DFM potentials with the DDM3Y effective interaction explain the elastic data over a large angular range where the cross section varies by roughly three decades.

The CDCC calculations exhibit generally an improved reproduction of the experimental data as compared to the single channel optical model calculations. This indicates the feedback and coupling of the breakup reactions, still present at higher projectile energies of 100A MeV, though reduced when compared with the lower energy effect.

A simplified phenomenological analysis of the breakup feature seen in the inclusive particle spectra shows that the ejectile momentum distributions do less depend from the target than noticed at low energies. This indicates a reduced orbital dispersion of the breakup particle in the field of the target nucleus. But since the results of differ-

ent authors show a large variety, it is difficult to reach a definite conclusion at this stage. Also the width of the observed longitudinal momentum distribution is larger than expected from the theoretical cluster wave function [2]. This may have several reasons, in particular, since the inclusive momentum distributions are affected by non-elastic breakup processes possibly leading to a broadening. Testing the intrinsic momentum distribution of the ^{6}Li projectile should concentrate to the *elastic* α-d breakup leaving the target nucleus (as catalyst) in the ground state. For that coincidence experiments are necessary.

In summary, the presented data are a basis for a simultaneous analysis of elastic scattering and breakup on equal footing. In order to enlarge this basis for an identification of the breakup channels of considerable influence, dedicated α-particle - deuteron coincidence experiments are in progress.

H.R., R.D., K.S. and C.S. sincerely acknowledge the kind hospitality of RCNP, Osaka. K.S. and C.S. thank the Japanese Ministry of Education, Science, Sports and Culture (Monbusho) for the support. K.S. additionally extends his gratitude to the German Academic Exchange Service (DAAD) for their assistance. C.S. also thanks the S.I.N.P., Calcutta and the RCNP, Osaka for encouraging this international collaboration. A part of this work was carried out with the Yamada Science Foundation award (C.S.).

References

1. G. Baur and H. Rebel, Ann. Rev. Nucl. and Part. Sc. **48**, 321 (1996)
2. Y. Sakuragi, M. Yahiro and M. Kamimura, Prog. Theor. Phys. Suppl. **89**, 136 (1986)
3. Y. Sakuragi, M. Ito, Y. Hirabayashi, and C. Samanta, Prog. Theor. Phys. (Letters) **98**, 521 (1997)
4. R. Kanungo, M. Lahiri, C. Samanta, and H. Rebel, Int. J. Mod. Phys. E **4**, 827 (1995)
5. G. R. Satchler and W. G. Love, Phys. Rep. **55**, 183 (1979)
6. R. Serber, Phys. Rev. **72**, 1008 (1947)
7. D. K. Srivastava, D. N. Basu, H. Rebel, and H. J. Gils, Z. Phys. A **335**, 417 (1990)
8. K. Van Bibber et al., Phys. Rev. Lett. **43**, 840 (1979)
9. H. Amakawa and K. I. Kubo, Nucl. Phys. A **266**, 521 (1976)
10. Y. Sakuragi, Phys. Lett. B **220**, 22 (1989)
11. Z. Majka, H.J. Gils, and H. Rebel, Phys. Rev. C **25**, 2996 (1982)
12. M. El-Azab Farid and G.R. Satchler, Nucl. Phys. A **438**, 525 (1985)
13. C. Samanta, Y. Sakuragi, M. Ito, and M. Fujiwara, Jour. Phys. G: Nucl. Part. Phys. **23**, 1697 (1997)
14. J.S. Al-Khalili and R.C. Johnson, Nuclear Physics A **546**, 622 (1992)
15. M. Yahiro, Y. Iseri, H. Kameyama, M. Kamimura, and M. Kawai, Prog. Theor. Phys. Suppl. **89**, 32 (1986)
16. A. Nadasen et al., Phys. Rev. C **47**, 674 (1993)
17. M. Fujiwara et al., Nucl. Instr. and Meth. in Phys. Res. A **422**, 484 (1999)
18. G. H. Rawitscher, Phys. Rev. C **9**, 2210 (1974)
19. M. Yahiro, M. Nakano, Y. Iseri and M. Kamimura, Prog. Theor. Phys. **67**, 1467 (1982)
20. M. Kamimura et al., Prog. Theor. Phys. Suppl. **89**, 1 (1986)
21. M. Kawai, Prog. Theor. Phys. Suppl. **89**, 11 (1986)
22. A. Ingemarsson and R. Shyam, Phys. Rev. C **60**, 054615 (1999)
23. G. Bertsch, J. Borysowicz, H. McManus, and W. G. Love, Nucl. Phys. A **284**, 399 (1977)
24. Z. Majka, H.J. Gils, and H. Rebel, Z. Phys. A **288**, 139 (1978)
25. J. Cook, H. J. Gils, H. Rebel, H. Klewe-Nebenius, and Z. Majka, Nucl. Phys. A **388**, 173 (1982)
26. R. Planeta et al., Nucl. Phys. A **448**, 110 (1986)
27. D. T. Khoa, G. R. Satchler, and W. von Oertzen, Phys. Rev. C **51**, 2069 (1995)
28. W. G. Love, T. Terasawa and G. R. Satchler, Nucl. Phys. A **291**, 183 (1977)
29. H. Jelitto et al., Z. Phys. A **332**, 317 (1989)
30. H. Rebel, D. K. Srivastava, KfK Report 4761, Forschungszentrum Karlsruhe (1990)
31. B. Neumann et al., Nucl. Phys. A **382**, 296 (1982)
32. H. Akimune et al., Phys. Rev. C **52**, 604 (1995)
33. A. S. Goldhaber, Phys. Lett. 53B, 306 (1974)
34. N. Heide, D. K. Srivastava, and H. Rebel, Phys. Rev. Lett. **63**, 601 (1989)